1   # Transgenic mouse facial nerve model of synkinesis

2   ## Original Research

3

4   Mostafa M Ahmed MD[1], Alexander Deich BA[2], Grace Balfour BA[1], Adrienne Laury MD[1],

5   Arkady Lorin MD[1], David Silliman BS[1], Richard L. Williams DMD, PhD[1]

6

7   [1]US Army Institute of Surgical Research, Ft Sam Houston, TX

8

9   [2]University of Illinois, Department of Physics, Urbana, IL

10

11

12

13   Corresponding Author (current address)

14   Mostafa Ahmed, MD

15   Department of Otolaryngology-Head and Neck Surgery

16   Carl Darnall Army Medical Center

17   36065 Santa Fe Ave

18   Fort Hood, TX 76544

19   Email: mmahm3d@gmail.com

20

22

23

24

25

26

27

28

29

30   Abstract:

31   Hypothesis: Our central hypothesis is that inhibition of Schwann cell de-differentiation,

32   in the post-injury setting, will reduce synkinesis and improve facial muscle function

33   Background: No therapies exist to improve the accuracy of facial nerve regeneration.

34   Following peripheral nerve injury, adult reactive Schwann cells de-differentiate and

35   express glial fibrillary acidic protein (GFAP); suggesting that reactive Schwann cells

36   impact axonal regeneration precision.

37

38   Methods: Transgenic GFAP-thymidine kinase (TK) mouse model was employed,

39   allowing selective downregulation of reactive GFAP expressing Schwann cells on

40   exposure of 7 day osmotic pump delivery of ganciclovir. Adult female transgenic GFAP-

41   TK mice had right facial nerve transected and then immediately repaired with tissue

42   glue, they then either were treated with saline or ganciclovir (GCV). At 6 weeks post-

43   injury, mice were exposed to random air puffs events while high speed videography

44   recorded whisker and eye movement. MatLab code video processing with publicly

45   available BIOTACT algorithm automatically tracked whiskers.

46   Results: Whisker velocity was calculated using binning statistical analysis. Saline

47   treated animals confirmed our model's ability to detect aberrant movement such that

48   intact (left) facial nerves caused whisker protraction, while repaired (right) facial nerves

49   had retraction. Administration of GCV increased whisker retraction compared to saline.

50   GCV did not impact intact animal whisker movement compared to repaired whiskers.

51

52   Conclusions: Inhibition of reactive Schwann cell proliferation appears to worse the

53   degree of synkinesis, providing important insight into a potential therapeutic target for

54   facial nerve injury.

55

56

57

58

59

60

61

62

63

64

65

66

67

68

69

70

71 **INTRODUCTION**

72 Facial nerve injury severely limits facial function typically resulting in weak facial

73 expressions and abnormal simultaneous mouth movement and eye closure or

74 synkinesis [1]. This aberrancy can occur either within the nerve fascicles itself or at the

75 facial muscle motor end-plates, resulting in the physiologic finding of synkinesis [2].

76 Despite advances in microsurgical techniques, complete nerve transection with primary

77 neurorrhaphy is classically believed to lead incomplete recovery with synkinesis.

78 A well-characterized model to study nerve reinnervation is the mouse femoral nerve

79 transection model[3]. In the femoral nerve model, there are two main branches re-

80 innervating motoneurons can follow, namely the motor branch or the cutaneous

81 (saphenous) branch. To investigate the role of neurotrophic factors on axonal guidance,

82 the transgenic GFAP-thymidine kinase (TK) mouse model was employed. GFAP is

83 expressed solely in reactive Schwann cells and not in uninjured Schwann cell

84 environments [3]. Adminstration of ganciclovir (GCV) ablates these reactive Schwann

85 cells. In the absence of end-organ contact (i.e., tie off distal cutaneous and muscle

86 branches), more motoneurons traveled down the cutaneous branch compared to the

87 motor branch. When examining potential causes for this preference, these authors

88 identified a 2-3-fold increase in reactive Schwann cell proliferation in the cutaneous

89 branch compared to the muscle branch following transection. This suggested that

90 Schwann cell proliferation plays a critical role in directing motoneuron reinnervation.

91 However, they noted, that after GCV application in transgenic GFAP-TK mice (resulting

92 in the removal of immature Schwann cells during reinnervation) this reinnervation

93 preference was eliminated [3]. Moreover, end-organ presence (i.e., patent distal

94   branches) with or without GCV resulted in motoneuron preference to the motor branch,

95   but still some cutaneous projections. These data argue that axonal pathway selectivity

96   is the result of a dynamic interaction between powerful attractant guidance cues

97   emanating from the end-targets as well as reactive Schwann cells lining the distal

98   pathway.

99   Transgenic mice, GFAP-TK in this case, have demonstrated promising results in

100   femoral nerve regeneration. Here we present our transgenic mouse facial nerve model

101   to study impact of Schwann cell on synkinesis following facial nerve injury and

102   immediate primary neurorrhaphy.

103   **METHODS**

104   *Nerve transection and drug delivery procedure*

105   This study was approved in accordance to the US Army Institute of Surgical Research

106   (ISR) IACUC protocol # A15-027. Sixteen 6-8 week old (22-27 g) female transgenic

107   GFAP-TK mice were obtained from Jackson Laboratory (stock #005698 Bar Harbor,

108   ME) [4]. Mice were anesthetized with an intraperitoneal injection of ketamine (80-100

109   mg/kg) and midazolam (4-5 mg/kg). Depth of anesthesia was monitored by a

110   combination of mechanical and observational monitoring techniques including but not

111   limited to: respiratory monitoring, response to stimulus, presence or absence of

112   movement during injury. Fur was removed from the right face and surgical field

113   sterilized. Under microscopic visualization, a post-auricular incision was made and blunt

114   dissection to the main trunk of right facial nerve was identified. Connective tissue was

115   freed from surround nerve. Sharp transection of the nerve at the apex of external

116   auditory canal was made. Fibrin sealant was immediately applied to tension free

117   apposition of nerve ends for anastomosis. The surgical bed was closed with absorbable

118   sutures and the animals were monitored according to ISR post-procedure protocol.

119   Osmotic pumps (Durect Inc, Cupertino, CA) filled either with saline or ganciclovir were

120   placed in a dorsal subcutaneous pocket. Based on nominal performance data from the

121   manufacturer we anticipate that fluid will be delivered at 0.5 µl/hr (± 0.1 µl/hr) allowing

122   for 7 day infusion.Ganciclovir (GCV) was dosed according to Madison et al 20

123   mg/kg/day diluted in saline. This dose is reported to kill any GFAP-TK expressing cells.

124   At one week animals were sedated to remove osmotic pumps.

125   *High-speed videography*

126   At six weeks post-operatively, the animals were imaged using high speed videography

127   at 500 frames per second using Fastec TS3 camera (Fastec, San Diego, CA) . The

128   camera was positioned directly overhead with lightsource positioned directly underneath

129   A puff of air was presented to the mouse snout positioned 3 cm from a measured and

130   standard puff delivered for 0.1 millisecond using AirStim system (San Diego

131   Instruments, San Diego, CA). Puffs were randomly delivered, to avoid habituation.

132   Using a modified conical tube, the body of the animal was restrained while the head

133   was freely mobile (figure 1). Videography data was analyzed using publicly available

134   MatLab code (Mathworks, Natick, MA) namely the BIOTACT Whisker Tracking Tool

135   (http://bwtt.sourceforge.net). Please refer to this URL to review how whisker position

136   was selected and extracted. Briefly, AVI files were uploaded to the BIOTACT program

137   and whisker position was calculated in radians in each frame. On the right side of

138   screen, animals left face, whisker protraction was represented with positive radian.

139   However, the left side of screen, animal's right face, whisker protraction was

140   represented with negative radians. Figure 2 illustrates the convention of whisker

141   movement.

142   In the GCV group, a total of 96 separate puffs were analyzed and a total of 111

143   separate puffs were analyzed in the saline group. Videos were manually annotated to

144   determine the exact moment eye closure began- marking the beginning at which nerve

145   impulse started to close the eye and move the whiskers. This provided the reference

146   point to which whisker movement was determined.

147   *Statistical analysis*

148   In order to compare the movement of one whisker run to another, we compared the

149   average velocity of the whiskers. This required solving two problems: One, the

150   resolution of the tracking software was not sufficient to track individual whiskers, and

151   adjacent whiskers were often confused. Two, it was not clear how long after the puff

152   the whisker motion was relevant to the question being studied. Too long after, and the

153   motion would be dominated by the stochastic motion which characterizes the whisker

154   motion in an ambient environment, and looking at too few post-puff frames would not

155   give sufficient data to extract reliable statistics.

156

157   *The resolution problem*

158   The tracking software we used to determine the whisker's trajectory would often

159   confuse two adjacent whiskers, especially when the two whiskers overlapped. This

160   meant that the position data was not reliable for any given whisker. However, the

161   tracking software was never in error by more than two adjacent whiskers, due to how

162   they're grouped on the mouse. This meant that while individual whiskers were

163   unreliable, we could bin the whisker trajectories, and tracking the mean position of a

164   given bin provided a reliable measure of the whiskers contained within that bin.

165

166   We found that binning with bins of 5 degrees enabled us to see useful features of the

167   whisker motion (pre- and post-puff stochasticity with a quiescent period immediately

168   post-puff) while also smoothing out the nonphysical tracking features.

169

170   *Determining the relevant data*

171   To determine how many frames post-puff we were interested in, we turned to a

172   mathematical technique called Fourier decomposition. What follows is a brief overview

173   of the technique and how we applied it.

174

175   Given any time-series signal (in our case, the position of a whisker over time), it is

176   possible to deconstruct that signal into a sum of pure sinusoidal waves different discrete

177   frequencies. By including more and more of these waves, it is possible to recreate a

178   signal to arbitrary precision. This provides a powerful tool: It is of general interest to the

179   physical sciences to be able to say what frequencies are most powerful for a given

180   signal.

181

182   By applying a Fourier decomposition to the whisker data, we were able to characterize

183   the motion of the whiskers in each phase of motion. In particular, by looking at which

184   frequencies were the most powerful at any given time, we were able to place a

185   statistical constraint on which frames were most relevant for velocity comparison. In

186   order to determine how many frames the initial post-puff phase lasts, we adopted the

187   following procedure: 1) Establish the peak of the frequency distribution (the Power

188   Spectral Density or PSD) before the puff (PSD_i). 2) Calculate the peak of the PSD for

189   increasing numbers of frames following the puff (PSD_f). 3) Calculate the magnitude of

190   the difference between these two numbers. As the number of frames increases, we

191   expect the PSD_f to diverge from PSD_i until some maximum difference, at which point

192   it will start to return to its previous stochastic motion, and the numbers begin to

193   converge.

194

195   When we perform this analysis, we find that this peak occurs at approximately frame 20

196   across all data runs. Fig. 4b shows an example of this analysis for one data run.

197

198   Having done this, we could extract the data from just those frames which immediately

199   followed the puff, and look at their average velocity in order to compare the motion of

200   whiskers from different data runs.

201

202

RESULTS

204   *High speed videography able to capture whisker response following puff stimulus*

205   At six weeks post-injury transgenic mice administered either saline or GCV were

206   recorded with high speed videography to determine if the Biotact algorithm was

207   sensitive enough to capture whisker movement. The raw data was expressed in radians

208   versus frame, with each frame being 1/500 seconds. Figure 3 is sample raw data from

209   saline treated animal.

210

211   *Determination of non-stochastic puff response time interval*

212   To evaluate the post-puff velocity behavior, we evaluate the whisker velocity in the 20

213   frames immediately following the puff. That number was determined by investigating

214   the average number of frames required for the whiskers to return to a pre-puff state.

215   Characterizing the pre-puff motion by looking at the distribution in frequency (known as

216   the power spectral density or PSD), we can compare the post-puff PSD (PSDf) with the

217   pre-puff PSD (PSDi) by making a simple subtraction and taking the average value. As

218   we increase the number of frames since the puff, this difference will grow as the

219   frequencies of the whisker movements experience a randomization period from the puff,

220   until they start to return to their pre-puff distribution. Thus, the difference in PSD pre-

221   and post-puff will show a peak. This is demonstrated for one data run in figure 4a. We

222   use this peak as the threshold to perform the velocity analysis, as this is the data which

223   will best capture the whisker behavior immediately after the puff, before it has returned

224   to its undisturbed (pre-puff) motion. Figure 4b shows the peak for all data runs, showing

225   that the peak occurs at 20.4 ± 3 frames. For simplicity, we take the value to be 20.

226

227

228   *GCV suppression increases synkinetic facial nerve function*

229   Following puff the normal facial nerve response is to simultaneously retract the whiskers

230   and close the eye. Calculating the velocity of whisker movement incorporates speed

231   and direction relative to the start of eye closure. Comparison between the intact and

232   repaired side therefore allows determination of synkinetic movement.

233   Following puff exposure, the intact side in both saline and GCV administered mice was

234   the same with a mean velocity (p=0.94) (Figure 5a) demonstrating GCV has no impact

235   on intact nerves. In the saline group, velocity response between intact (-0.24 rad/s,

236   protraction) and repaired (0.34 rad/s, retraction) sides was statistically different (p<0.05)

237   (figure 5b). In the GCV group, velocity response between intact and repaired sides was

238   statistically different, such that the right side (mean value of 4.3 rad/s, retraction) is

239   significantly different from the left (mean value -1.2 rad/s, protraction) (p<0.001) (figure

240   5C). Comparison between saline and GCV groups on the injured side demonstrated

241   mean velocity of 3.2 rad/s (retraction) with GCV treatment versus saline treatment

242   velocity 0.8 rad/s (retraction) (p<0.05) (figure 5D).

243   **DISCUSSION**

244   In this study we administered GCV to mice with the transgenic mutation of GFAP-TK to

245   suppress post-injury Schwann cell proliferation. Our main finding is that reactive

246   Schwann cell proliferation increases synkinetic action. The basis of this study was

247   derived from work by Madison et al where they describe following sciatic nerve injury,

248   adult reactive Schwann cells de-differentiate and re-express glial fibrillary acidic protein

249   (GFAP) [3].

250   Defining facial nerve synkinesis is a matter of understanding normal facial nerve

251   function. In the rodent, facial nerve function dictates eye lid and whisker position [5].

252   Following puff exposure, the intact side responded with eyelid closure and whisker

253   protraction. In the injured side, retraction was seen with eyelid closure representing

254   synkinesis. Suppression of reactive Schwann cells appears to worsen facial nerve

255   recovery, suggesting that they play a key role in regeneration accuracy.

256   Here we capture facial nerve function with minimal modification to animal itself.

257   Additionally, high spatiotemporal videography (ie 500 frames per second) allowed for

258   large amount of data pertaining to simultaneous eyelid and whisker position. Estimation

259   of error in calculation of whisker position was minimal at 500 frames per second [6].

260   The main weakness of our study is the lack of histologic confirmation of GCV

261   suppression of reactive Schwann cell response and success of regeneration through

262   anastomosis and at the muscle end-plates. Additionally, various repair methods other

263   than tissue glue could have been compared. Lastly, tracking temporal change in facial

264   nerve function before and beyond 6 weeks could elucidate progressive worsening or

265   improvement of facial nerve function.

266   In conclusion, this study develops the first transgenic mouse model to study synkinesis.

267   We demonstrate, the pharmacologic suppression of Schwann negative impact on facial

268   nerve function. The benefit of using a mouse model, is the vast number of genetic

269   mutations that can be targeted for parallel, high through-put post-injury and therapy

270   screening of molecular targets.

271

272

273

274

275

276

277

278

279

280

281

282

283

284

285

286

287

288

289   References

290   1.   Hadlock T, Kowaleski J, Lo D, et al. Functional assessments of the rodent facial
291   nerve: a synkinesis model. *Laryngoscope*. 2008;118(10):1744-1749.
292   doi:10.1097/MLG.0b013e31817f5255

293   2.   Seitz M, Grosheva M, Skouras E, et al. Poor functional recovery and muscle

294   polyinnervation after facial nerve injury in fibroblast growth factor-2-/- mice can be
295   improved by manual stimulation of denervated vibrissal muscles. *Neuroscience.*
296   2011;182:241-247. doi:10.1016/j.neuroscience.2011.03.032

297   3.   Madison RD, Sofroniew M V, Robinson GA. Schwann cell influence on motor
298   neuron regeneration accuracy. *Neuroscience.* 2009;163(1):213-221.
299   doi:10.1016/j.neuroscience.2009.05.073

300   4.   Bush TG, Puvanachandra N, Horner CH, et al. Leukocyte infiltration, neuronal
301   degeneration, and neurite outgrowth after ablation of scar-forming, reactive
302   astrocytes in adult transgenic mice. *Neuron.* 1999;23(2):297-308.
303   http://www.ncbi.nlm.nih.gov/pubmed/10399936.

304   5.   Kaya Y, Ozsoy U, Turhan M, Angelov DN, Sarikcioglu L. Hypoglossal-facial nerve
305   reconstruction using a Y-tube-conduit reduces aberrant synkinetic movements of
306   the orbicularis oculi and vibrissal muscles in rats. *Biomed Res Int.*
307   2014;2014:543020. doi:10.1155/2014/543020

308   6.   Perkon I, Kosir A, Itskov PM, Tasic JF, Diamond ME. Unsupervised quantification
309   of whisking and head movement in freely moving rodents. *J Neurophysiol.*
310   2011:jn.00764.2010. doi:10.1152/jn.00764.2010

311

312

313

314

315

316

317

318

319

320

321

322

323

324

325   Figure 1: Animal positioning with top-down high-speed videography

326

327   Figure 2: Convention of whisker movement

328

329   Figure 3: Raw whisker data with puff initiation marked

330

331   Figure 4a: Power spectral density distribution

332

333   Figure 4b: Power spectral density difference demonstrating post-puff peak

334

335   Figure 5a: Velocity response on intact side (left) after puff

336

337   Figure 5b: Velocity response with saline treatment

338

339   Figure 5c: Velocity response with GCV treatment

340

341   Figure 5d: Velocity comparison between saline and GCV treatment on injured side
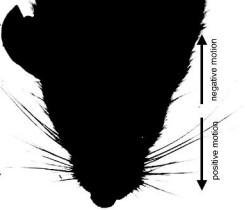
342

343

344

345